Synthesis, DFT study and photoelectrical characterizations of the novel 4-methoxyfuro[3`,2`:6,7]chromeno[2,3-e]benzo[b][1,4]diazepin-5(12H)-one

Article *in* Optik - International Journal for Light and Electron Optics · April 2018

DOI: 10.1016/j.ijleo.2018.04.001

CITATIONS
0

READS
16

5 authors, including:

Magdy Ahmed Ibrahim
Ain Shams University
77 PUBLICATIONS **412** CITATIONS

SEE PROFILE

Shimaa Abdel Halim Hussien
Ain Shams University
16 PUBLICATIONS **10** CITATIONS

SEE PROFILE

N. Roushdy
24 PUBLICATIONS **201** CITATIONS

SEE PROFILE

Alaa Farag
Ain Shams University
135 PUBLICATIONS **1,799** CITATIONS

SEE PROFILE

Optik 166 (2018) 294–306

Contents lists available at ScienceDirect

Optik

journal homepage: www.elsevier.de/ijleo

Original research article

Synthesis, DFT study and photoelectrical characterizations of the novel 4-methoxyfuro[3‘,2‘:6,7]chromeno[2,3-e]benzo[b][1,4]diazepin-5(12H)-one

Magdy A. Ibrahim [a], Shimaa Abdel Halim [a], N. Roushdy [b], A.A.M. Farag [c,d,*], Nasser M. El-Gohary [a]

[a] Department of Chemistry, Faculty of Education, Ain Shams University, Roxy, 11711, Cairo, Egypt
[b] Electronics Materials Dep., Advanced Technology & New Materials Research Inst., City of Scientific Research & Technological Applications (SRTA-City), New Borg El-Arab City, P.O. Box: 21934 Alexandria, Egypt
[c] Physics Department, Faculty of Science and Arts, Jouf University, Jouf, Saudi Arabia
[d] Thin Film Laboratory, Physics Department, Faculty of Education, Ain Shams University, Roxy, 11711, Cairo, Egypt

ARTICLE INFO

Article history:
Received 1 February 2018
Received in revised form 1 April 2018
Accepted 1 April 2018

Keywords:
Annulated visnagin
FT-IR spectrum
TD-DFT theoretical investigation
Polarizability
Hyperpolarizability
Phototransient properties

ABSTRACT

Condensation reaction of 6-formylvisnagin (**1**) with *o*-phenylenediamine afforded the novel 4-methoxyfuro[3‘,2‘:6,7]chromeno[2,3-*e*]benzo[*b*][1,4]diazepin-5(12*H*)-one (**MFCBD**). Hypothetical examination for the harmony geometries of the recently synthesized MFCBD has been done by Density Functional Theory (DFT) at the B3LYP/6-311G (d,p). The TD-DFT computations were explored for the electronic absorption spectra which the measured in polar and nonpolar solvents. The spectrophotometer measurements of both transmittance and reflectance in the range of 200–2500 nm were used for obtaining the significant optical constants. The optical absorption coefficient was analyzed to obtain the type of transition and found to be directly allowed with energy gaps of 1.1 and 2.93 eV. The dispersion parameters were extracted on the basis of the single oscillator mode using Wemple-DiDomenico and Selemier relationships. The dark and illuminated current density-voltage characteristics of the **MFCBD**-based heterojunction showed rectifying property which may be due to the formation of the organic/inorganic interface. The obtained phototransient current confirms the sensibility of the prepared heterojunction to the light illumination of 100 mW/cm^2. The results support the applicability for the heterojunction in the field photodiode application.

1. Introduction

Khellin(4,9-dimethoxy-7-methyl-5*H*-furo[3,2-g]chromen-5-one) is considered to be the major noteworthy constituent of the plant Ammi visnaga [1,2], and has the variable biological activity such as antiatherosclerotic and lipid-altering activity [3], treating psoriasis and vitiligo [4–6]. Generally, furochromones have anti-inflammatory and analgesic [7–9], antitumor [10], antimicrobial [11], anticancer activities [12].

* Corresponding author at: Thin Film Laboratory, Physics Department, Faculty of Education, Ain Shams University, Cairo, Egypt.
E-mail addresses: alaafaragg@gmail.com, aamfaraj@ju.edu.sa (A.A.M. Farag).

https://doi.org/10.1016/j.ijleo.2018.04.001
0030-4026/

DFT-theoretical calculation can be investigating the optimized geometries of the synthesized compound; 4-methoxyfuro[3',2':6,7]chromeno[2,3-*e*]benzo[*b*][1,4]diazepin-5(12*H*)-one (**MFCBD**). Also, study the dipole moment, atomic charge FT-IR, equilibrium geometries, harmonic vibrational frequencies, thermo-chemical parameters, and energetic of the molecule. Some of the main important parameters like the linear polarizability $\langle\Delta\alpha\rangle$, and first order hyperpolarizability $\langle\beta\rangle$ are required for the rational design of optimized materials for several applications [13,14].

The TD-DFT is a quantum mechanical hypothesis utilized as a part of material science and science to research the properties and elements of many-body frameworks within the sight of time-subordinate possibilities, for example, electric or attractive fields. The effect of such fields on molecules can be mulled over with TD-DFT to extricate highlights like excitation energies and frequency-dependent response properties [15]. This computation was used to examine the extremity of solvent on the observed spectra and hence explain the observed electronic transitions bands. Furochromone derivatives like MFCBD behaves as semiconductor materials and showed a remarkable optical sensitivity to light and applicability for the optoelectronic application. Accordingly, these types of materials-based devices are specifically designed to improve the light absorption and emission, resulting in a high conversion efficiency [16,17].

In continuation to our previous study for the synthesis and characterizations of furochromone [arag, the present work is devoted to investigating the reactivity of 6-formylvisnagin towards *o*-phenylenediamine hoping to prepare of a new derivative of annulated visnagin **MFCBD** [16–18].

The morphological attributes of the examples are researched by utilizing checking by scanning electron microscopy. Furthermore, the optical characteristics are resolved by applying the single-oscillator model to extract the significant dispersion parameters. The type and the value of optical energy gap are also estimated Also, photoluminescence and optical film absorption are interested to examine the applicability of the device based **MFCBD**–heterojunction for optoelectronic applications.

2. Experimental

2.1. Preparation and molecular structural characterizations of MFCBD

A mixture of carboxaldehyde **1** (1.08 g, 4 mmol) and *o*-phenylenediamine (0.42 g, 4 mmol), in ethanol (20 mL) was re reflux for 30 min. The obtained orange-red crystals were filtered and recrystallized from DMF/MeOH to produce compound **2** as orange crystals. Yield (0.47 g, 71%), m.p. 281–282 °C. IR (KBr, cm^{-1}): 3429 (NH), 3120 (CH_{furan}), 3040 (CH_{arom}), 2938, 2875 (CH_{aliph}), 1665 ($C{=}O_{\gamma\text{-pyrone}}$), 1588 (C=N and C=C). ^{1}H-NMR (400 MHz, DMSO-d_6): 3.95 (s, 3 H, OCH_3), 6.76 (s, 1 H, H-14), 7.10–7.18 (m, 4 H, Ar-H), 7.24 (d, 1 H, H-$3_{furan,}$ J = 2.0 Hz), 7.78 (d, 1 H, H-$2_{furan,}$ J = 2.0 Hz), 8.53 (s, 1 H, CH=N), 9.83 (bs, 1 H, NH). Mass spectrum, *m/z* (I_r %): 332 (M^+, 39), 319 (14), 303 (27), 275 (11), 246 (5), 190 (18), 176 (14), 147 (45), 132 (23), 119 (43), 108 (74), 91 (32), 77 (40), 64 (100). Anal. Calcd for $C_{19}H_{12}N_2O_4$ (332.32): C, 68.67; H, 3.64; N, 8.43%. Found: C, 68.50; H, 3.45; N, 8.25%.

A digital Stuart SMP3 apparatus (Büchi, Flawil, Switzerland) was used to determine the melting point of **MFCBD**. FTIR Nicolet IS10 spectrophotometer (cm^{-1}) (Thermo Fisher Scientific, USA) was used to measure infrared spectra, using KBr disks. ^{1}H NMR spectra (400 MHz) and ^{13}C NMR (100 MHz), were measured on Mercury-400BB(Bruker, Rheinstetten, Germany), using DMSO-d_6 as a solvent and TMS (δ) as the internal standard. Mass spectrum was obtained using GC-2010 Shimadzu Gas chromatography instrument mass spectrometer (70 eV) (Manchester, England). Elemental microanalyses were performed on a Perkin-Elmer CHN-2400 analyzer (Leco, St. Joseph, USA) at the Chemical War Department, Ministry of Defense, Egypt. The chemical reagents used were purchased from E. Merck (Darmstadt, Germany) and 4-methoxy-5-oxo-5*H*-furo[3,2-*g*]chromene-6- carboxaldehyde (**1**) was prepared according to the literature [19].

2.2. Computational method

DFT Khon-Sham's method calculations were done at B3LYP method [15,20,21]. The Gaussian 09 package was selected for optimizing the geometry [22] and GaussView 5.0.9 [23] or Chemcraft 1.6 [24] software packages by this function [20] at the 6-311G (p,d) bases set [21]. FT-IR vibrational spectra of (**MFCBD**) based on the computationally predicted assignments. The total static dipole moment values were also considered [25–27].

2.3. Thin film preparation and physical characterizations of MFCBD

Successful layers of **MFCBD** were fabricated on various types of substrates with high quality by utilizing a type 306 Auto. The thickness of the prepared films was controlled through measurement from the condition of the preparation with the average value of ~300 nm. After the preparation procedures, the microstructural characteristics of the films were examined by applying the scanning electron microscope (SEM). Optical measurements were achieved by using JASCO–670 spectrophotometers in the range of 200–2500 nm. Measurements of electrical characteristics of the heterojunction were employed by an electrometer type Keithly 2635 A in dark and under illumination.

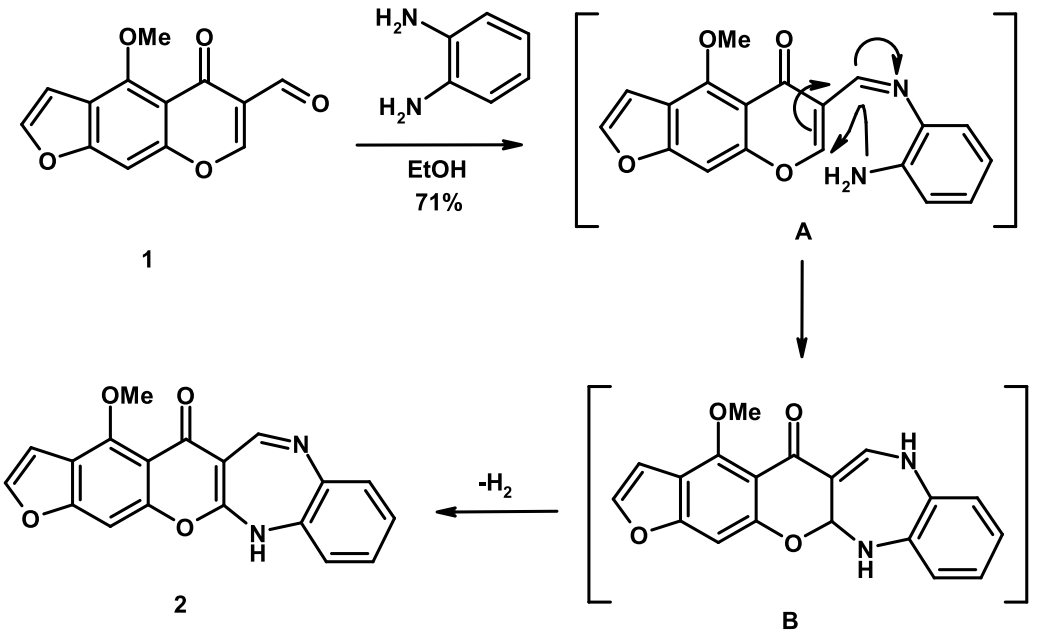

Fig. 1. Formation of the novel MFCBD.

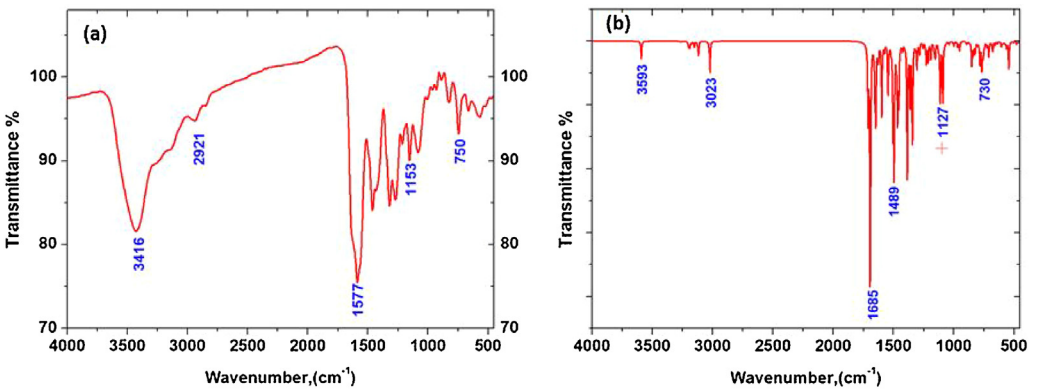

Fig. 2. (a) Experimental IR spectrum and (b) theoretical IR spectrum at B3LYP/6-311G (d,p). of MFCBD.

3. Results and discussion

3.1. Molecular structure and reaction confirmation

Herein, the condensation of carboxaldehyde **1** with 1,2-phenylenediamine in ethanol afforded 4-methoxyfuro[3',2':6,7]chromeno[2,3-*e*] benzo[*b*][1,4]diazepin-5(12*H*)-one (**MFCBD**) in 71% yield. The reaction may proceed through the formation of the corresponding Schiff base intermediate **A** (nonisolable) followed by an intramolecular nucleophilic addition at the C-7 position leading to intermediate **B** which underwent self-oxidation under the reaction condition producing the final product **2** as depicted in Fig. 1. IR spectrum (Fig. 2(a)) showed the characteristic absorption bands at 3429 (NH), 3120 (CH_{furan}), 3040 (CH_{arom}), 2938, 2875 ($C\,H_{aliph}$), 1665 ($C{=}O_{\gamma\text{-pyrone}}$), 1588 cm^{-1} (C=N and C=C). The ^{1}HNMR spectrum of the compound showed the characteristic singlet signals assigned to OCH_3, H-14, and CH=N at δ 3.95, 6.76 and 8.53, respectively. In addition to D_2O-exchangeable signal at δ 9.83 which refers to NH proton. The mass spectrum of **MFCBD** showed the parent ion peak at *m/z* 332 corresponding to the suggested molecular formula ($C_{19}H_{12}N_2O_4$) and supports the structure.

The comparison of the computational vibrational frequencies at B3LYP/6-311G (d,p) with those for experimental one are listed in (Table 1) and (Fig. 2(b)). Another attempt to follow up the changes of the studied compound **MFCBD** is carried out by studying vibrational spectra. The Assignment could be achieved extensively as in the following: The aromatic C—H stretching vibrations [28,29] is in general observed in the region 3000–3100 cm^{-1}. The computed vibration is assigned

Table 1
The Optimized calculations of total energies (a.u.), Zero point vibrational energies (kcal·mol^{-1}), Rotational constants (GHz), Entropies (cal·k^{-1}), energy of HOMO and LUMO (eV), energy gap (eV) and total dipole moment (Debye) for **(MFCBD)** at the B3LYP/6-311 G(d,p).

Parameters	**MFCBD**
Total Energy,(E_T)	−1141.87994647
Zero Point Vibrational Energy	171.58158
	0.56273
Rotational constant	0.11980
	0.10276
Total Entropy	142.823
Translational	43.296
Rotational	35.094
Vibrational	64.433
Energy of highest occupied molecular orbital (E_{HOMO})	5.786528
Energy of lowest unoccupied molecular orbital (E_{LUMO})	1.80064
Energy Gap,(E_g)	3.985888
Dipole moment, (μ)	5.3085

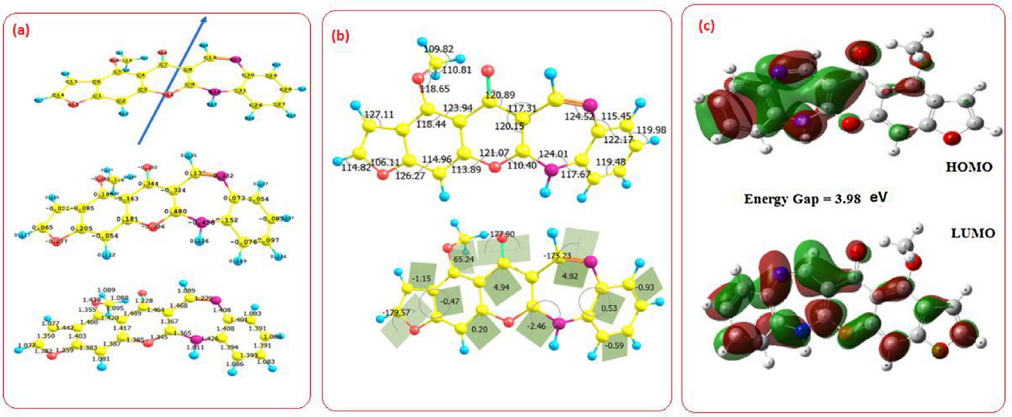

Fig. 3. (a) Optimized geometry, numbering system, net charge, vector of dipole moment and bond length, (b) Bond angle and dihedral angle, and (c) HOMO and LUMO for 4-methoxyfuro[3',2':6,7]chromeno[2,3-e] benzo[b][1,4]diazepin-5(12 H)-one (MFCBD).

to asymmetric C—H aromatic stretching vibrations at 3127 cm^{-1} for compound **MFCBD** which is comparable with those for the experimental. The computed vibration is assigned to symmetric C—H aliphatic stretching vibration in CH_3 at 3152 and 3023 cm^{-1} respectively for **MFCBD** has shown a comparable agreement with the experimental one. The computed vibration is assigned to twisting C—H furan stretching vibration at 3261 cm^{-1} for compound **MFCBD** which has shown a comparable agreement with the experimental result. The computed vibration is assigned to N—H asymmetric vibration at 3592 cm^{-1} for compound **MFCBD** which has shown a comparable agreement with experimental results at 3429 cm^{-1}. Generally, the C=O vibrations [30] is observed in the region 1790–1810 cm^{-1}. Vibrations are assigned to asymmetric C=O stretching at 1694 cm^{-1} for compound **MFCBD** which is comparable agreement with experimental results at 1665 cm^{-1}. The band of C=C vibrations is detected in the 1480–1630 cm^{-1} region [29]. The computed vibration is assigned to C=C and C=N stretching vibrations at 1598 cm^{-1} for compound **MFCBD** which is comparable with experimental results at 1588 cm^{-1}.

3.2. Molecular orbital calculations of the ground state energy

The optimized geometries, the vector of the dipole moment and the net charges of **MFCBD** obtained using the B3LYB/6-311G (p,d) level are given in (Fig. 3(a–c)). The ground state energies are listed in Table 2. The analysis of (Table 2) and (Fig. 3(a–c)) show that: The optimized bond length of C=C in phenyl ring falls in the range from 1.350 to 1.489 A° which are in great matching with that experimental one [29] for C=O bonds the optimized length obtained by B3LYB/6-311G (p,d) is slightly shorter than the experimental data 1.229A° [29] The computed bond angles are largely affected by the presence of C=O group in C7, especially $<N_{36}C_9O_{12}$, $<C_{19}N_{25}C_{30}$ and $<C_4C_7O_{11}$ are respectively at 110.40°, 124.52° and 120.89°. The most stable geometry of the studied compound **MFCBD** is the planar structure, except methoxy moiety and diazepin moiety (where the dihedral angle is between 0.00° and 180°). The active centers O and N of **MFCBD** show a significant change in the Mullikan net charge so; indicating that the interaction between different moieties of **MFCBD**. The ionization energy (I.E.) of **MFCBD** is 5.78 eV (Table 2). Also, the electron affinity (E.A.) of **MFCBD** is 1.80 eV. So the calculated energy gaps, (E_g), is

Table 2
Experimental and computational calculated vibrational wave-numbers (harmonic frequency (cm^{-1})), IR intensities and assignments for compound **MFCBD** at the B3LYP/6-311 G (d,p).

No.	Exp.	Wave number		IR Intensity		Assigments	References
		unscaled	scaled	Rel.	Abs.		
1	3429	3592	3485	40.53	51.09	υ N-H	
2	3120	3261	3189	2.11	4.23	υ C-H furan	[28]
3	3040	3127	3110	4.66	8.25	υ C-H aromatic	
4	2938, 2875	3152	3023	4.76	72.18	υ C-H aliphatic	
5	1665	1694	1676	546.96	320.35	υ C=O γ-pyrone	[29]
6	1588	1598	1579	167.43	97.35	β C=N Asym and C=C (in ring)	

υ (Stretching); υ_2(Symmetric stretching); υ_3(Asymmetric stretching); β (In plane bending).

Table 3
Total static dipol moment (**μ**), the mean polarizability (<**α**□), the anisotropy of the polarizability (**Δα**), and the mean first-order hyperpolarizability (<**β**□), for **MFCBD** by B3LYP/6-311 G (d,p).

Property	PNA	B3LYP/6-311G(d,P)
μ_x		−1.0738677Debye
μ_y		−1.1583947Debye
μ_z		−1.3663625Debye
μ	2.44 Debye [a]	2.088544134Debye
α_{XX}		385.570768a.u.
α_{XY}		−35.9991135a.u.
α_{YY}		231.681579a.u.
α_{ZZ}		−25.3751693a.u.
α_{YZ}		54.6931218a.u.
α_{XZ}		137.3093511a.u.
<α>	22×10^{-24} cm[3b]	37.27×10^{-24} esu
Δα		36.87×10^{-24} esu
βxxx		105.5726 a.u.
βxxy		−31.9382 a.u.
βxyy		1.7219 a.u.
βyyy		−30.1167 a.u.
βxxz		60.1331 a.u.
βxyz		11.5320a.u.
βyyz		15.9420 a.u.
βxzz		16.4360 a.u.
βyzz		6.4622 a.u.
βzzz		−2.3533 a.u.
<β>	15.5×10^{-30} esu[c]	94.87×10^{-30} esu

[a, b, c] PNA results are taken from references [34–40].

3.98 eV (≈92 kcal). Finally, the theoretically computed dipole moment (μ) is 5.31 D, the value of ZPVE is 171.581 kcal mol^{-1} and total entropy is 142.823 cal k^{-1} (Table 1).

3.3. *Polarizability and hyperpolarizability*

Polarizabilities and hyperpolarizabilities characterizing the reaction of the system under influence of electric field [31]. They locate not only the quality of atomic associations and additionally the cross-areas of various diffusing and crash forms yet, in addition, the non-linear optical (NLO) properties [32,33]. the connections of photocurrent time, atomic structures, and NLO explored the polarizabilities and hyperpolarizabilities of the title compound were computed utilizing B3LYP technique, 6–311 G (d,p) premise set, in view of the limited field approach. The mean hyperpolarizability ⟨β⟩, the static dipole minute (μ), the mean polarizability (<α□), and the anisotropy of the polarizability (Δα), of title atom, are displayed in Table 3. The figured estimation of dipole minute was observed to be 2.08854 D at B3LYP/6-311G (d,p). The computed mean polarizability (<α□) is 37.27×10^{-24} esu i.e. two times higher than PNA particle. Moreover, the figured mean initially arrange hyperpolarizability $\langle \beta \rangle$, of the structure and found to be 94.87×10^{-30} esu (c.f. Table 3). This outcome demonstrates the linearity of the title particle and promising the title atom to be utilized as NLO materials. In this examination, the run of the mill NLO material, P-nitroaniline (PNA) is one of the prototypical particles was picked as a source of perspective atom; in light of the fact that there were no trial esteems about the title compound in the writing. In this manner, it was utilized every now and again as a limit an incentive for relative purposes and still keeps on being a perceived model of natural NLO chromophores.

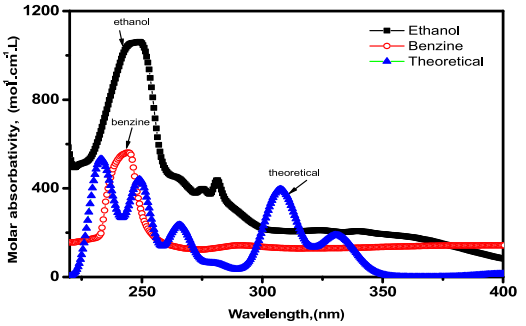

Fig. 4. Electronic absorption spectra of MFCBD.

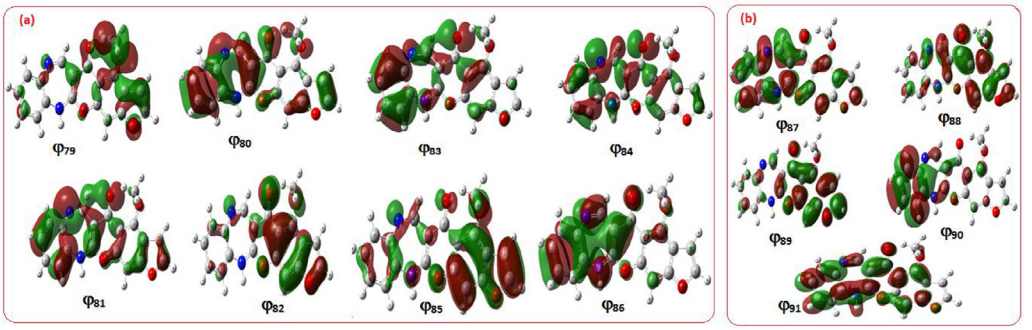

Fig. 5. (a) The charge density maps of the occupied MO's, (b) The charge density maps of the unoccupied MO's of compound (MFCBD).

Its hyperpolarizability was considered both tentatively and hypothetically in different solvents and at various frequencies [34–40].

3.4. Electronic absorption spectra of MFCBD

Assignment of the electronic spectra of **MFCBD** in ethanol and benzene are given in Fig. 4 and Table 3. The charge thickness maps of the involved and empty MO,s considered in the advances are introduced in Fig. 4(a). The spectrum in benzene is composed of six bands centered at 315.37 nm, 288.82 nm, 257.79 nm 242.96 nm, 240.83 and 238.46. Increasing solvent polarity ongoing from benzene to ethanol causes small changes in band positions indicating that the polarity of the excited and ground state are of the same values, that is, solvent independent. The intensity is lowered in the case of ethanol as compared to other solvents. All the bands are assigned to (π-π^*) transitions as reflected from their intensities (200–1300). The excited configurations considered in **MFCBD** are those which results from an electron excitation of eight highest occupied molecular orbital's $\varphi_{79}{}^{-1}\varphi_{86}$ and the lowest five vacant molecular orbital's $\varphi_{87}{}^{-1}\varphi_{91}$. The correspondence between the hypothetically figured and the experimentally observed transitions are satisfactory.

The first (π-π^*)^1 state is centered at 315.37 nm in benzene. This band is predicted theoretically at 307.76 nm, which is in good agreement with the experimental one. and has configurations namely, $\varphi_{84}{}^{-1}\varphi_{87}$, $\varphi_{85}{}^{-1}\varphi_{87}$, and $\varphi_{86}{}^{-1}\varphi_{88}$. This band is characterized by a delocalizing band and charge transfer from furo-chromone moiety to the benzodiazepine moiety. The second (π-π^*)^1 state is observed at 288.82 nm in benzene and is predicted theoretically at 265.61 nm which is considered to be collected from a mixture of eight configurations, (Table 3) (i.e. CT, localized and delocalized configurations may be expected). The main contribution of this band is coming from the two configurations $\varphi^{-1}{}_{82}\,\varphi_{87}$ and $\varphi^{-1}{}_{84}\,\varphi_{88}$, which is of CT character from furo-chromone moiety to the benzodiazepine moiety and delocalized. The third (π-π^*)^1 state is observed in benzene at 257.79 nm and is predicted theoretically at 249.33 nm. This band is composed of a mixture of ten configurations and assigned as a delocalized and CT character from furochromone moiety to the benzodiazepine moiety and localized transition (Table 3). The fourth (π-π^*)^1 state is theoretically computed at 236.71 nm and observed in benzene at 242.96 nm. This band is composed of six configurations, namely, $\varphi^{-1}{}_{79}\,\varphi_{88,}$ $\varphi^{-1}{}_{80}\,\varphi_{87,}$ $\varphi^{-1}{}_{81}\,\varphi_{88}$, $\varphi^{-1}{}_{81}\,\varphi_{90,}$ $\varphi^{-1}{}_{84}\,\varphi_{90}$ and $\varphi^{-1}{}_{85}\,\varphi_{90}$. This band is CT character from furo-chromone moiety to the benzodiazepine moiety, delocalized and localized bands (Fig. 5(a) and (b)). The fifth (π, π^*)^1 state computed at 240.83 nm in benzene, 235.19 nm in ethanol and is theoretically computed at 233.75 nm as listed in Table 4. This state has high polarity in comparison with those for the ground state and consequently, then the solvent dependence on the band position is predictable. This state is composed of a mixture of eight configurations, that is also assigned as a delocalized and a charge transfer band (CT) from furo-chromone moiety to the benzodiazepine moiety. The last one state computed theoretically, appears at 229.98 nm. This state is composed of a

Table 4
Calculated band maxima and intensities of compound **MFCBD** by TD method.

State	Theoretical					Experimental	
	Configuration	Coefficient	λ, nm	f	Type	Polar λ, nm	Non polar λ, nm
I	84–87	−0.26443	307.76	0.2838	π–π*	310.02	315.37
	85–87	0.59995			π–π*		
	86–88	0.20466			π–π*		
II	81–88	0.19355	265.61	0.1701	π–π*	276.04	288.82
	82–87	0.43626			π–π*		
	83–87	0.23224			π–π*		
	83–88	0.32617			π–π*		
	84–87	−0.11062			π–π*		
	84–88	−0.18160			π–π*		
	85–88	−0.12272			π–π*		
	86–90	0.15526			π–π*		
III	81–87	0.38118	249.33	0.2847	π–π*	251.94	257.79
	81–88	0.11223			π–π*		
	82–87	0.14804			π–π*		
	82–88	−0.24397			π–π*		
	83–87	−0.21906			π–π*		
	83–88	−0.10482			π–π*		
	84–89	0.15463			π–π*		
	85–89	0.10361			π–π*		
	86–90	−0.30603			π–π*		
	86–91	−0.13867			π–π*		
IV	79–88	−0.11303	236.71	0.1148	π–π*	238.73	242.96
	80–87	−0.12342			π–π*		
	81–88	0.20335			π–π*		
	81–90	−0.11536			π–π*		
	84–90	0.45085			π–π*		
	85–90	0.40791			π–π*		
V	79–87	0.11380	233.75	0.1704	π–π*	235.19	240.83
	79–88	0.40961			π–π*		
	80–87	0.12684			π–π*		
	81–87	−0.11333			π–π*		
	82–88	−0.29515			π–π*		
	84–89	−0.10923			π–π*		
	85–89	0.32535			π–π*		
	85–90	0.11285			π–π*		
VI	79–87	0.11179	229.98	0.1245	π–π*	232.53	238.46
	79–88	0.14140			π–π*		
	80–88	0.14586			π–π*		
	82–88	0.19459			π–π*		
	84–90	−0.37442			π–π*		
	85–90	0.46394			π–π*		

mixture of six configurations, both states are π-π* and assigned as a delocalized, CT character from furo-chromone moiety to the benzodiazepine moiety and localized transition.

3.5. SEM characterizations

Morphological representation of our samples by Images from Scanning electron microscopy (SEM) is observed in Fig. 6(a) and (b). The observed images show the morphology of the **MFCBD** samples, elucidating the infrequently crystallite size allocation and highly accumulated grains. Furthermore, the basic structure shows microrodes-like morphology and there are some very fine-grained (nanoparticles) grown over the micro-rodes have most probably the same structure of **MFCBD**. The average particle size by using the particle size analyzer is found to be about 600 nm(Fig. 6(c)). Higher grain size is appropriate for photovoltaic applications due to the lower grain boundaries [41].

3.6. Optical characterizations of MFCBD thin films

Fig. 7(a) depicts the behavior of both transmittance (T) and reflectance (R) of the films as a function of wavelength. The presence non-shrinking interference fringes confirm the homogeneity and smooth properties of **MFCBD** films [42]. Furthermore, the films are characterized by a highly transparent in the visible range and the transmission reaches up to 90% at 2500 nm. Moreover, the edge of absorption in the UV region can firstly be calculated by taking the derivative of T with

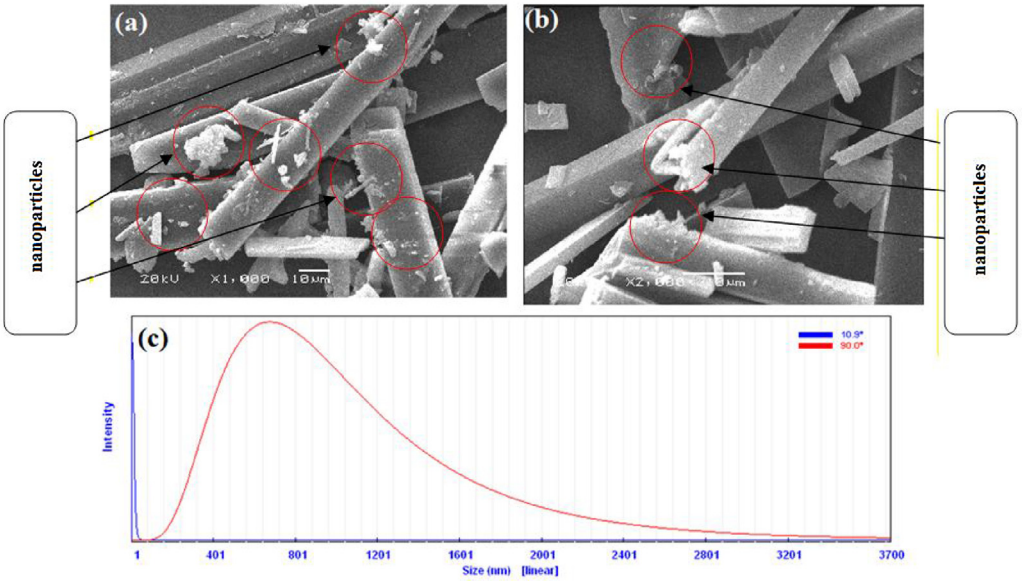

Fig. 6. SEM of different magnifications (a) 1000×, (b) 5,000, (c) and (d) particle size analysis.

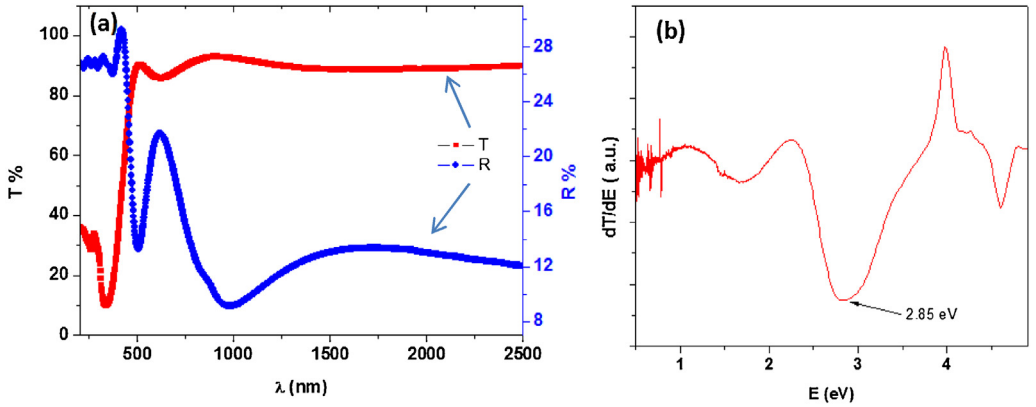

Fig. 7. (a) Spectral dependence of T and R characteristics, (b) Plot of dT/dE vs. E of MFCBD thin films.

respect to the photon energy (E) (i.e. $\frac{dT}{dE}$), as discussed by Al-Kuhaili et al.[43] and shown in Fig. 7(b). the obtained energy gap value of **MFCBD** films is found to be 2.85 eV.

The expression of the absorption coefficient(α) as a function of photon energy for obtaining the energy gap, E_g according to the direct transition is as follows [42]:

$$(\alpha h\nu)^2 = K\left(h\nu - E_g\right) \tag{1}$$

where the parameter K is a constant. The value of E_g of the **MFCBD** films is calculated from the optical absorption measurements by fitting the absorption coefficient data to the above equation. Fig. 8(a) and (b) shows the best fit of $(\alpha h\nu)^2$ vs. $(h\nu)$ in the ultraviolet and visible regions. The value of E_g can be obtained from the intercept of the fitting linear part to $(\alpha h\nu)^2 = 0$. The results show that the values of E_g are found to be 1.1 and 2.93 eV for the visible and visible regions, respectively. The latter value of energy gap is in agreement with those obtained from the photon energy dependence of $\frac{dT}{dE}$. The band edges position of the junction structure were theoretically predicted using the empirical equation of atom's mullikan electronegativity [44–46]. Accordingly, the calculated CB (E_{CB}) and VB (E_{VB}) edge position for the heterojunction could easily be and compared with those obtained experimentally. The discrepancy between the values of the process and calculated theoretically in the presence of interactions between molecules due to the fact that the accounts actually conducted in one part a single molecule in the gaseous state.

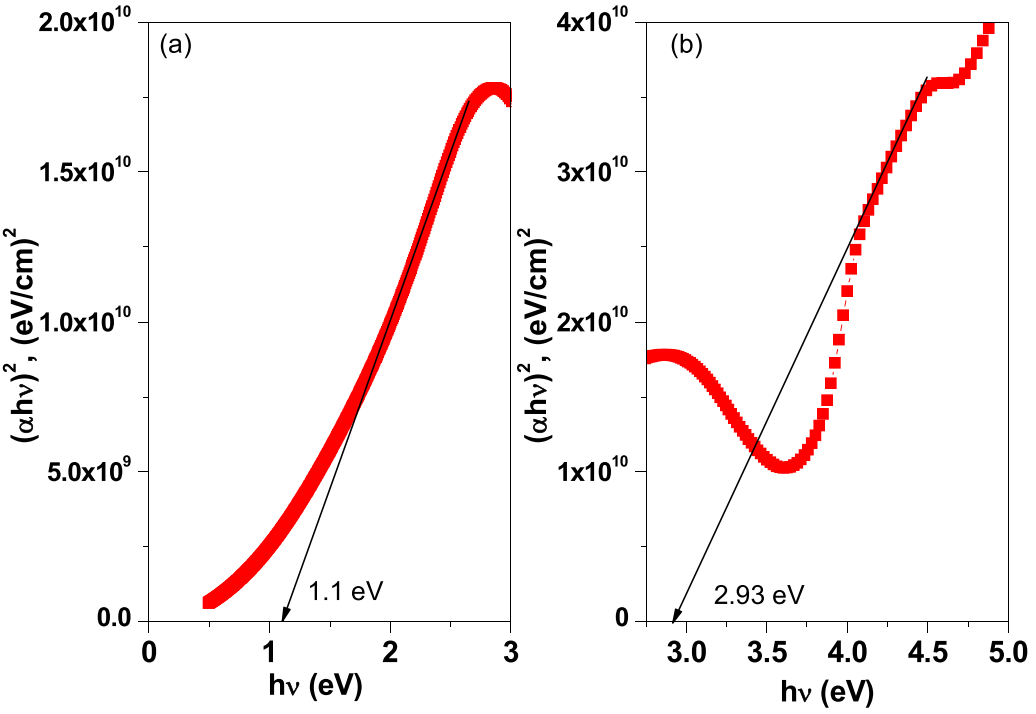

Fig. 8. Plot of $(\alpha h\nu)^2$ vs. $h\nu$ of (a) region I and (b) region II for MFCBD thin films.

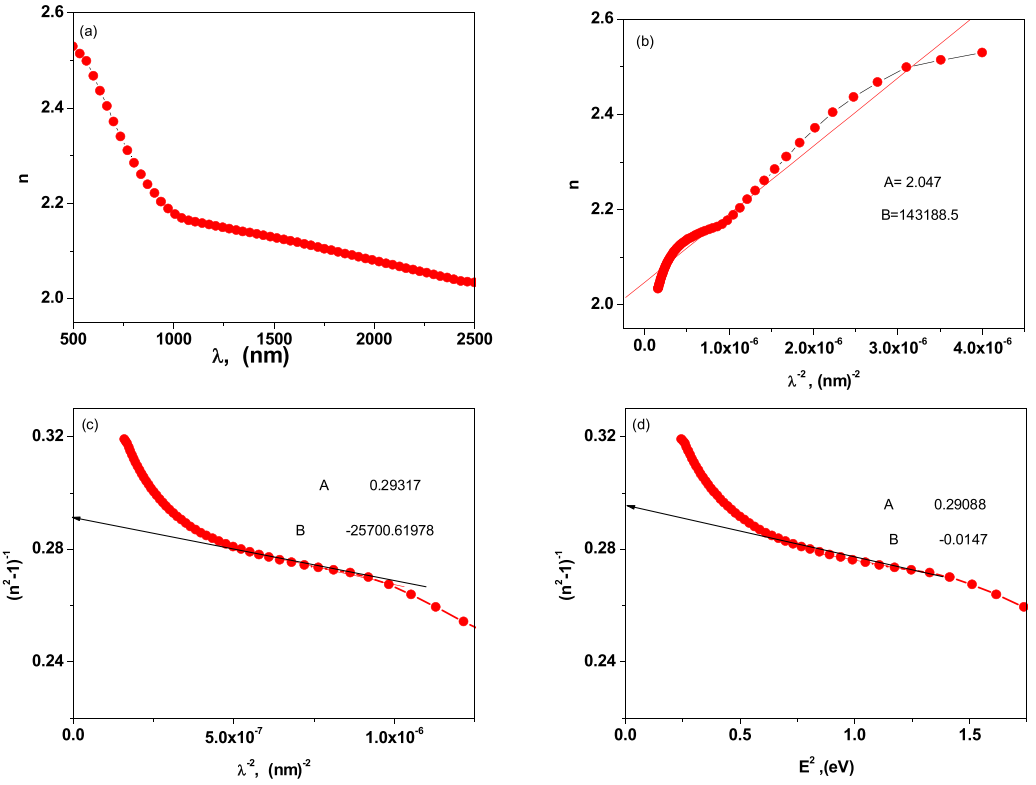

Fig. 9. (a) Plot of n vs. λ, (b) Plot of n vs. λ^{-2}, (c) Plot of $(n^2\text{-}1)^{-1}$ vs. λ^{-2} and (d) Plot of $(n^2\text{-}1)^{-1}$ vs. E^2 for MFCBD thin films.

The results of refractive index can be fitted according to the single oscillator model in the region of non-absorbing, where the refractive file diminishes with expanding wavelength as appeared in Fig. 9(a). The dispersion of the refractive index, n can obey the well-known Cauchy dispersion equation as follows [47]:

$$n(\lambda) = A + \frac{B}{\lambda^2} \tag{2}$$

where A and B are the characteristic Cauchy parameters of the material. The Cauchy parameters A and B are estimated from the graphical reorientation of n versus λ^2 as shown in Fig. 9(b) and found to be 2.047 and 1.4×10^5 nm^2, respectively. The obtained values of Cauchy parameters are in agreement with those published for most semiconductors [48,49]. Skuban et al. [47] announced that the parameter A indicates n_∞. They also reported that the Cauchy equation is limited for obtaining an obvious physical meaning for the parameters but it is only used for describing the refractive index dispersion.

The Sellmeier model is proposed for obtaining a well-known described parameters in the non-absorbing region as follows [50]:

$$(n^2 - 1)^{-1} = \frac{1 - \left(\lambda_0/\lambda\right)^2}{S_0 \lambda_o^2} \tag{3}$$

where S_0 is the average oscillator strength, and λ_0 is the wavelength oscillation. Fig. 9(c) illustrates the graphical representation of $(n^2\text{-}1)^{-1}$ versus $1/\lambda^2$ for **MFCBD** films and fitted using the above equation and the values of S_0 and λ_0 are found to be 3.8×10^{13} m^2 and 300 nm.Another dispersion relation for the single oscillator model proposed by Wemple and DiDomenico as follows [51]:

$$(n^2 - 1)^{-1} = \frac{E_0}{E_d} - \left(\frac{1}{E_0 E_d}\right) E^2 \tag{4}$$

where E is the phonon energy and E_0 is the oscillator strength (i. e. parameter related to the electric dipole oscillator strength), E_d is the dispersion energy (i.e. related to the effective dispersion [52]. The values of E_0 and E_d are obtained from the slope and intercept of the linear fit of the above equation using the results of Fig. 9(d) and found to be 15.3 and 4.44 eV, respectively. The latter parameter is also related to the average energy gap of the material and comparable with those obtained from the above theoretical calculations.

3.7. Current density-voltage characteristics

The *J–V* measurements of **MFCBD**/p-Si heterojunctions, measured at 300 K is represented in Fig. 10(a). The outcomes affirm that the heterojunction acts a diode-like because of the arrangement of the boundary at the interface. Thus, the higher value of the forward current as compared to the reverse one which provides the rectification characteristics with a rectification ratio of 5.4 at ± 1.75 V as represented in Fig. 10(b). The essential parameters of the heterojunctions are the series resistance (R_s) and shunt resistance (R_{sh}). Firstly the value of R_s can be determined from the part of the *J–V* characteristics at which the current deviates from linearity due to the effect of R_s. Fig. 11(a) shows the dependence of the current versus the voltage drop at the terminal of the J–V characteristics and then the R_s can easily be determined using the inverse of the slope of this curve. The determined R_s is found to be 2.8 kΩ. Fig. 11(b) shows the variation of junction resistance versus bias voltage (Rj) (i.e. $\partial V/\partial J$) as discussed by Sharma et al. [53]. The series resistance (R_s) and R_{sh} can be obtained at sufficient high forward and reverse voltages, respectively. The obtained values of R_s and R_{sh} are found to be 2.47 and 13.7 kΩ, respectively.

Furthermore, the **MFCBD**/p-Si heterojunction (HJ) shows good rectifying characteristics under illumination of 100 mW/cm^2 as shown in Fig. 12(a). It is well known that the forward biased current under illumination and increases with increasing the intensity of the incident light intensity. Continuously, the reverse biased current also increases with illumination which is the requirement for the production of exciton followed by the generation of the charge carriers at the HJ interface [53].

To realize the conduction mechanism of the studied heterojunction, the transient photocurrent study is considered. Fig. 12(b), shows that the photocurrent of the heterojunction increases under the effect of illumination of 100 mW/cm^2 the device and return to its initial value after the illumination is turning off the. This confirms the sensitivity of the presented heterojunction to the effect of the illumination and then a candidate for photodiode application. Moreover, the mechanism of increasing the current due to the effect of illumination can be attributed to the photo-carrier that contributing to the current. When the light is turning off, a decrease in the generation of carriers and then the current decreases. The obtained results are compared with those obtained by Farag et al. [18] for BFCMT/ p-Si. They found that these type of structure suggests a high absi\orption coefficient and considerable sensitivity for the effect of illumination wich supports the studied structure for most organic-based photovoltaic applications

4. Conclusion

In conclusion, condensation of 6-formylvisnagin (**1**) with 1,2-phenylenediamine in ethanol afforded the novel 4-methoxyfuro[3',2':6,7]chromeno[2,3-*e*]benzo[*b*][1,4] diazepin-5(12*H*)-one (**MFCBD**). The electronic absorption spectra

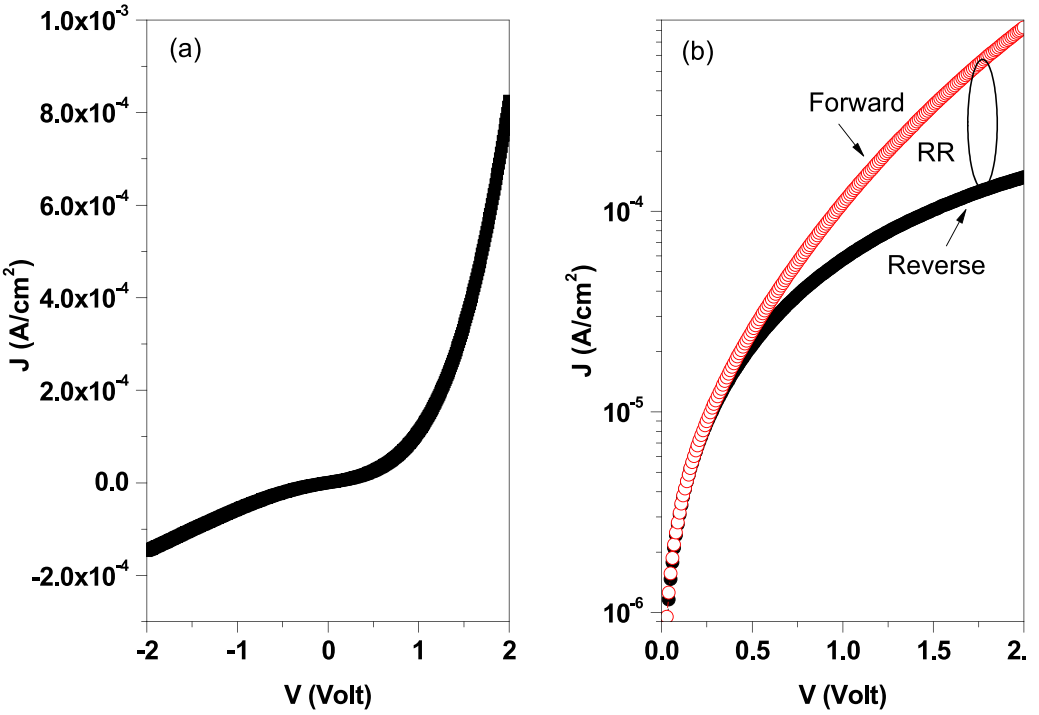

Fig. 10. (a) Plot of J vs. V and (b) Plot of semilogarithmic J vs. V for MFCBD /p-Si heterojunction.

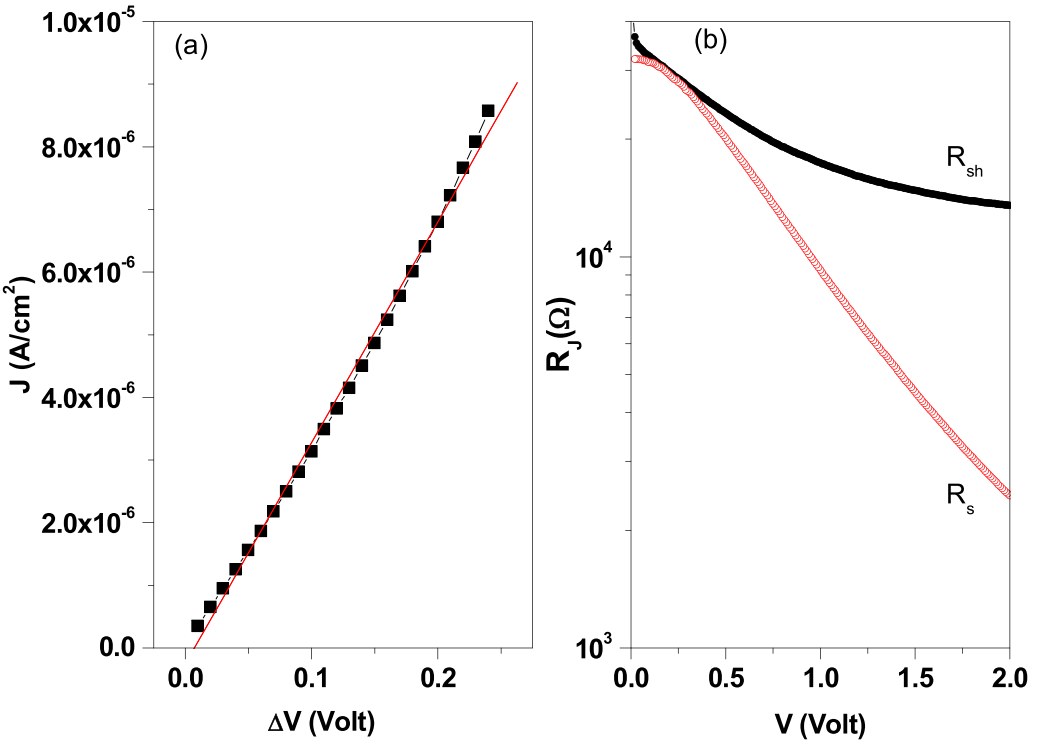

Fig. 11. (a) Plot of J vs. ΔV and (b) Plot of R_J vs. V for MFCBD/p-Si heterojunction.

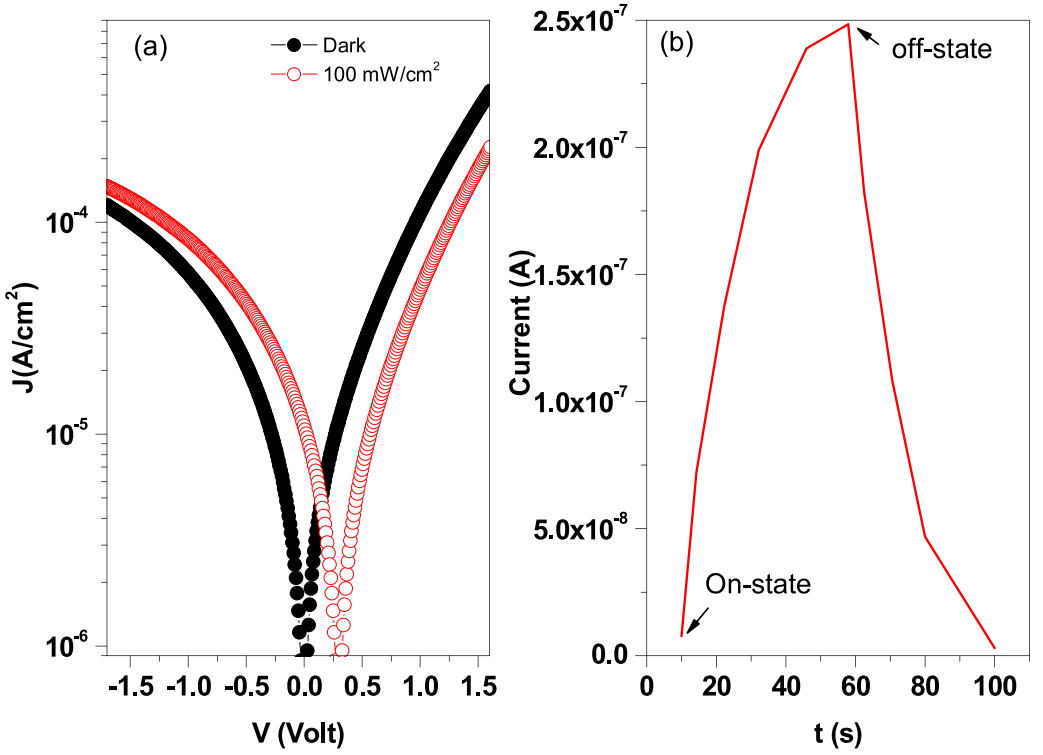

Fig. 12. (a) Plot of J vs. V in dark and under illumination of 100 mW/cm^2 and (b) Plot of J vs. t for MFCBD/p-Si heterojunction.

carried out by TD-DFT calculation. All the observed bands can be assigned to (π-π^*) transitions as reflected from their intensities. The results of the theoretically computed and the experimentally observed transitions are good. The dipole moments of ground and excited states are the solvent dependence of the observed bands. The FT-IR spectrum of **MFCBD** is recorded in the solid phase. The calculated dipole moment, polarizability, and first-order hyperpolarizability results indicate that the structure has a reasonable good non-linear optical behavior. Two direct permitted optical band gaps were acquired and observed to be 1.1 and 2.93 eV. The electrical characteristics showed rectification characteristics. Moreover, the main extracted electrical parameters are found to be respectively 2.47 and 13.7 kΩ for R_s and R_{sh}. The phototransient current properties of the **MFCBD**-based heterojunction under influence of 100 mW/cm^2 was recorded which give chance for the prepared heterojunction for light photodetector application.

References

[1] R. Pavela, N. Vrchotová, J. Tříska, Exp. Parasitol. 165 (2016) 51–57.
[2] A.A. Abu-Hashem, M. El-Shazly, Eur. J. Med. Chem. 90 (2015) 633–665.
[3] R.B. Gammill, C.E. Day, P.E. Schurr, J. Med. Chem. 26 (1983) 1672–1674.
[4] D. Vedaldi, S. Caflleri, F. Dall'Acqua, L. Andrea, L. Bovalini, P. Martelli, Farmaco 4 (1988) 333–346.
[5] B.E. Cohen, N. Elbuluk, E.W. Mu, S. Orlow, J. Am. J. Clin. Dermatol. 16 (2015) 463–474.
[6] L. Trabalzini, P. Martelli, L. Bovalini, F. Dall'Acqua, E. Sage, J. Photochem. Photobiol. B: Bid 7 (1990) 317–336.
[7] M. Ghate, M.V. Kulkarni, Indian J. Chem. 44B (2005) 1674–1678.
[8] M.S. Frasinyuk, S.V. Gorelov, S.P. Bondarenko, V.P. Khilya, Chem. Heterocycl. Compd. 45 (2009) 1261–1269.
[9] A.A. Abu-Hashem, M.M. Youssef, Molecules 16 (2011) 1956–1972.
[10] I.F. Zaeid, A.M. Nasef, N.M. Fawzy, A.M. Soliman, M.M. El-Baroudy, Int. J. Pharm. Sci. Rev. Res. 30 (2015) 306–314.
[11] H. Regaila, A. Gohar, G. Abdel Sadek, Egypt. J. Pharm. Sci. 29 (1988) 343.
[12] A.S. Abd El-All, S.A. Osman, H.M.F. Roaiah, A.A. Abd El Aty, W.H. Abdel-Hady, Med. Chem. Res. 24 (2015) 4093–4104.
[13] P.N. Prasad, D.J. Williams, Introduction to Nonlinear Optical Effects in Molecules and Polymers, John Wiley & Sons, New York, NY, USA, 1991.
[14] F. Meyers, S.R. Marder, B.M. Pierce, J.L. Brédas, J. Am. Chem. Soc. 116 (1994) 10703.
[15] (a) A.D. Becke, J. Chem. Phys. 98 (1993) 5648–5652;
(b) A.D. Becke, J. Chem. Phys. 98 (1993) 1372–1377.
[16] N.M. El-Gohary, Magdy A. Ibrahim, Eslam R. El-Sawy, N.A. Abdel-Fatah, J. Heterocycl. Chem. 54 (2017) 1467–1478.
[17] Magdy A. Ibrahim, T.E. Ali, A.M. El-Kazak, A.M. Mohamed, J. Heterocycl. Chem. 52 (2015) 815–826.
[18] A.A.M. Farag, M.A. Ibrahim, S. Abdel Halim, N. Roushdy, N.M. El-Gohary, J. Mol. Struct. 1156 (2018) 516–523.
[19] F. Eiden, J. Schünemzinn, Arch. Pharm. 316 (1983) 201–208.
[20] (a) C. Lee, W. Yang, R.G. Parr, Phys. Rev. B Condens. Matter. 37 (1988) 785–789;
(b) B. Miehlich, A. Savin, H. Stolt, H. Preuss, Chem. Phys. Lett. 157 (1989) 200–206.
[21] B.B. Stefanov, G. Liu, A. Liashenko, P. Piskorz, I. Komaromi, R.L. Martin, D.J. Fox, T. Keith, M.A. Al-Laham, C.Y. Peng, A. Nanayakkara, M. Challacombe, P.M.W. Gill, B. Johnson, W. Chen, M.W. Wong, C. Gonzalez, J.A. Pople, Gaussian 03, Revision B.03, Gaussian, Inc., Pittsburgh PA, 2003.
[22] M.J. Frisch, G.W. Trucks, H.B. Schlegel, G.E. Scuseria, et al., Gaussian 09, Revision C.01, Gaussian, Inc., Wallingford, CT, 2009.

[23] R. Dennington, T. Keith, J. Millam, GaussView, Version 5, Semichem Inc., Shawnee Mission, KS, 2009.
[24] http://www.chemcraftprog.com.
[25] D. Avci, Spectrochim. Acta A 82 (2011) 37–43.
[26] D. Avci, A. Başoğlu, Y. Atalay, Struct. Chem. 21 (2010) 213–219.
[27] D. Avci, H. Cömert, Y. Atalay, J. Mol. Model. 14 (2008) 161–170.
[28] T.J. Bednarchuk, V. Kinzhybalo, O. Bednarchuk, A. Pietraszko, J. Mol. Struct. 1120 (2016) 138–149.
[29] J.B. Lambert, H.F. Shurvell, L. Vereit, R.G. Cooks, G.H. Stout, Organic Structural Analysis, Academic Press, New York, 1979.
[30] P.S. Kalsi, Spectroscopy of Organic Compounds, Academic Press, New York, 2002.
[31] C.R. Zhang, H.S. Chen, G.H. Wang, Chem. Res. Chin. Univ. 20 (2004) 640–646.
[32] Y. Sun, X. Chen, L. Sun, X. Guo, W. Lu, Chem. Phys. Lett. 38 (2003) 397–403.
[33] O. Christiansen, J. Gauss, J.F. Stanton, Chem. Phys. Lett. 305 (1999) 147–155.
[34] L. Jensen, P.T. Van Duijnen, J. Chem. Phys. 123 (2005) 074307.
[35] P. Sałek, O. Vahtras, T. Helgaker, H. Ågren, J. Chem. Phys. 117 (2002) 9630.
[36] M. Stähelin, D.M. Burland, J.E. Rice, Chem. Phys. Lett. 191 (1992) 245–250.
[37] F.L. Huyskens, P.L. Huyskens, A.P. Persoons, J. Chem. Phys. 108 (1998) 8161–8171.
[38] L.T. Cheng, W. Tam, S.H. Stevenson, G.R. Meredith, G. Rikken, S.R. Marder, J. Phys. Chem. 95 (1991) 10631–10643.
[39] S.P. Karna, P.N. Prasad, M. Dupuis, J. Chem. Phys. 94 (1991) 1171–1181.
[40] P. Kaatz, E.A. Donley, D.P. Shelton, J. Chem. Phys. 108 (1998) 849–856.
[41] A. Yildiz, S. Uzun, N. Serin, T. Serin, Scr. Mater. 113 (2016) 23–26.
[42] E.R. Shaaban, Y.A.M. Ismail, H.S. Hassan, J. Non-Cryst. Solids 376 (2013) 61–67.
[43] M.F. Al-Kuhaili, S.M.A. Durrani, A.S. El-Said, R. Heller, J. Alloys Compd. 690 (2017) 453–460.
[44] S. Selvarajan, A. Suganthi, M. Rajarajan, M.M. Shrividhya, Optik 153 (2018) 16–30.
[45] S. Selvarajan, A. Suganthi, M. Rajarajan, K. Arunprasath, Powder Technol. 307 (2017) 203–212.
[46] S. Selvarajan, P. Malathy, A. Suganthi, M. Rajarajan, J. Ind. Eng. Chem. 53 (2017) 201–212.
[47] F. Skuban, S.R. Lukić, D.M. Petrović, I.O. Gúth, J. Non-Cryst. Solids 355 (2009) 2059–2062.
[48] C.S. Huang, C.Y. Liu, W.C. Su, Mater. Sci. Semicond. Proc. 80 (2016) 302–323.
[49] D. Prakash, E.R. Shaaban, M. Shapaan, S.H. Mohamed, A.A. Othman, K.D. Verma, Mater. Res. Bull. 80 (2016) 120–126.
[50] W. Yang, Z. Zhou, B. Yang, Y. Jiang, H. Tian, D. Gong, H. Sun, W. Chen, Appl. Surf. Sci. 257 (2011) 7221–7225.
[51] S.H. Wemple, M. DiDomenico, Phys. Rev. B 3 (1971) 1338–1351.
[52] G.D. Sharma, P. Balaraju, S.K. Sharma, M.S. Roy, Synth. Met. 158 (2008) 620–629.
[53] N.S. Kumar, M.S. Raman, J. Chandrasekaran, R. Priya, M. Chavali, R. Suresh, Mater. Sci. Semicond. Proc. 41 (2016) 497–507.